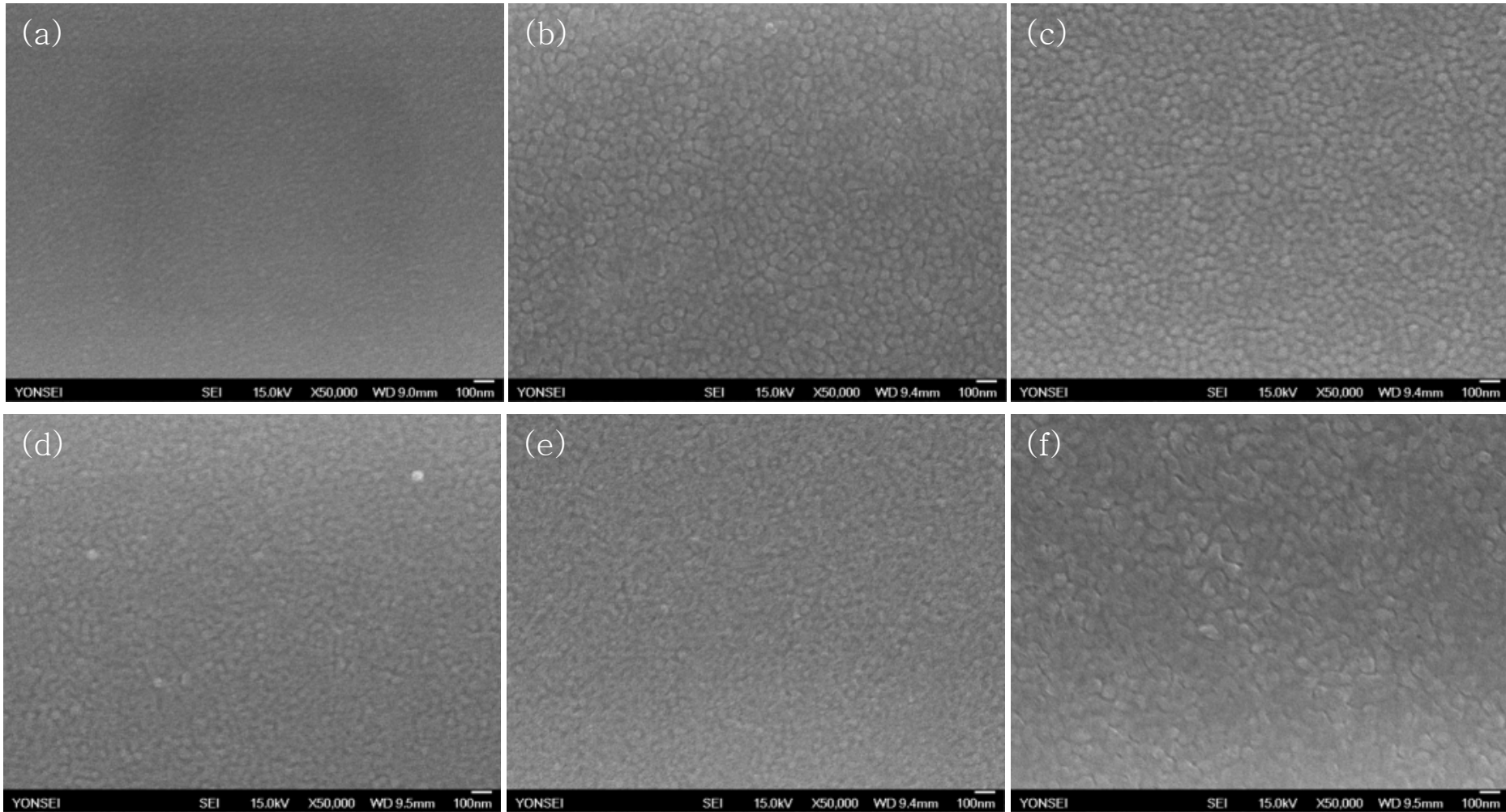


Electronic Supplementary Information

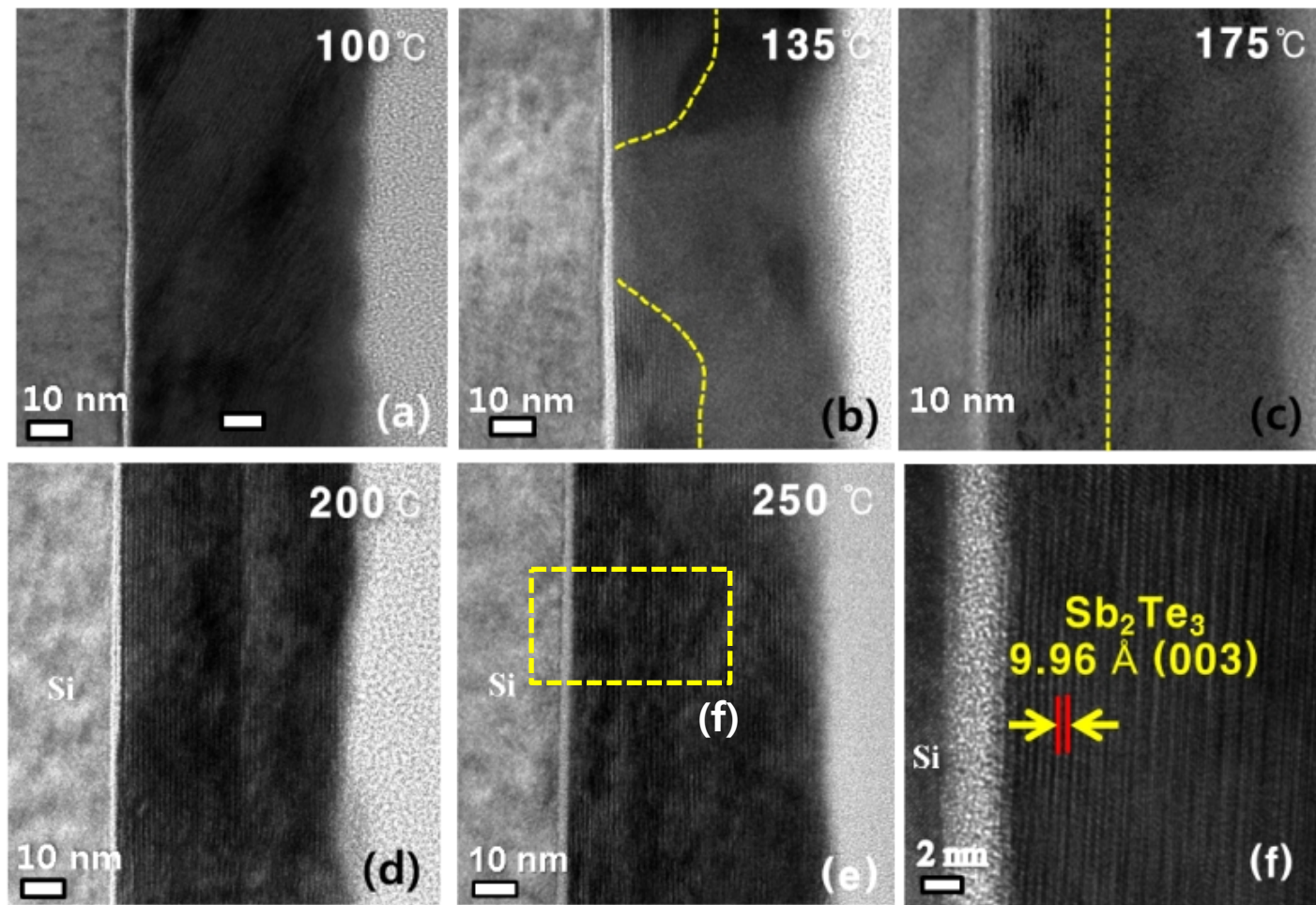
Title : Enhancement of carrier lifetime by spin-orbit coupling in a topological insulator of a Sb_2Te_3 thin film

Supporting information S1.



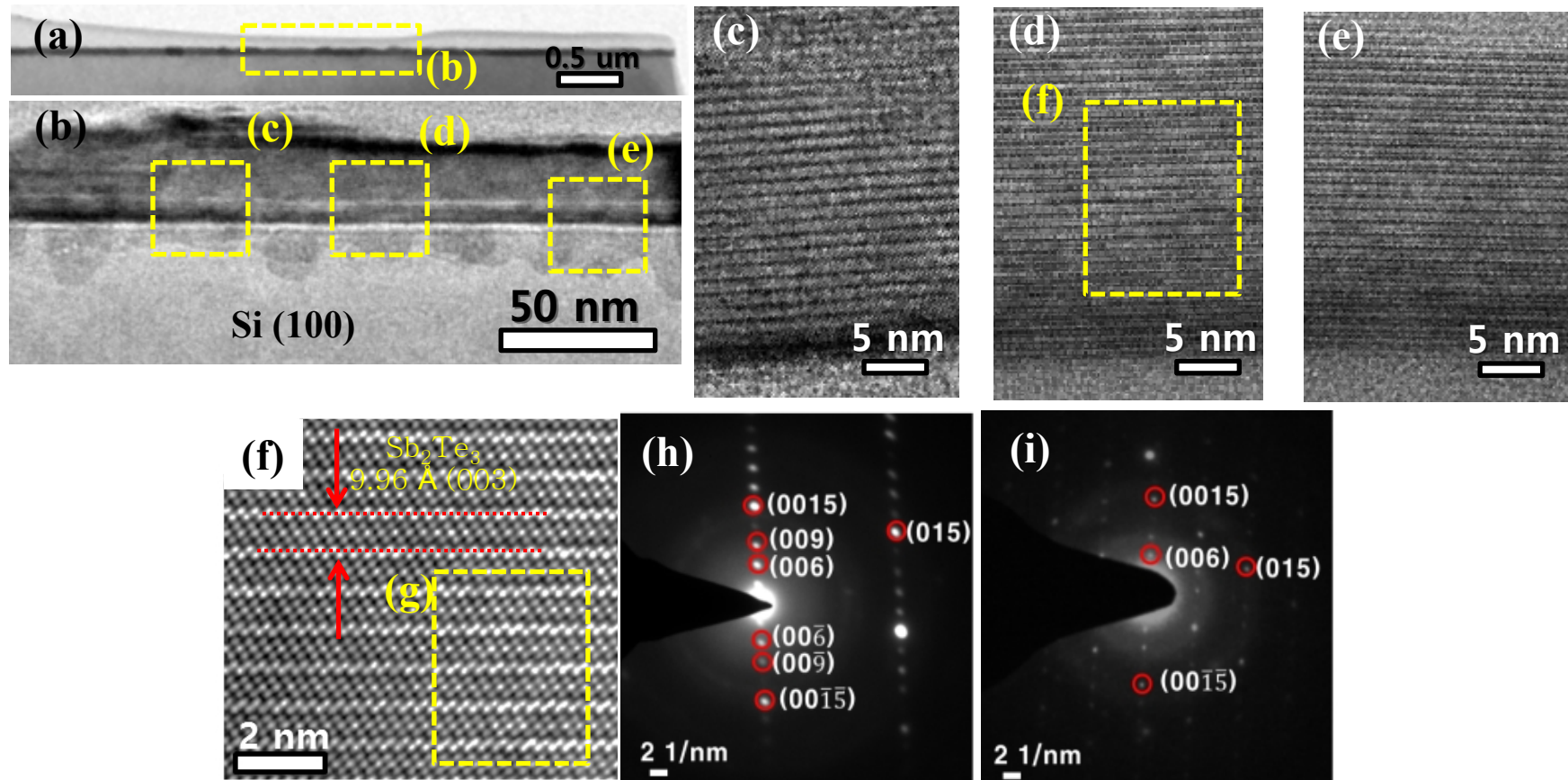
Supporting information S1. SEM images of (a) as-grown, (b) 135 °C annealed , (c) 150 °C annealed
(d) 175 °C annealed (e) 200 °C annealed and (f) 220 °C annealed thin film.

Supporting information S2.



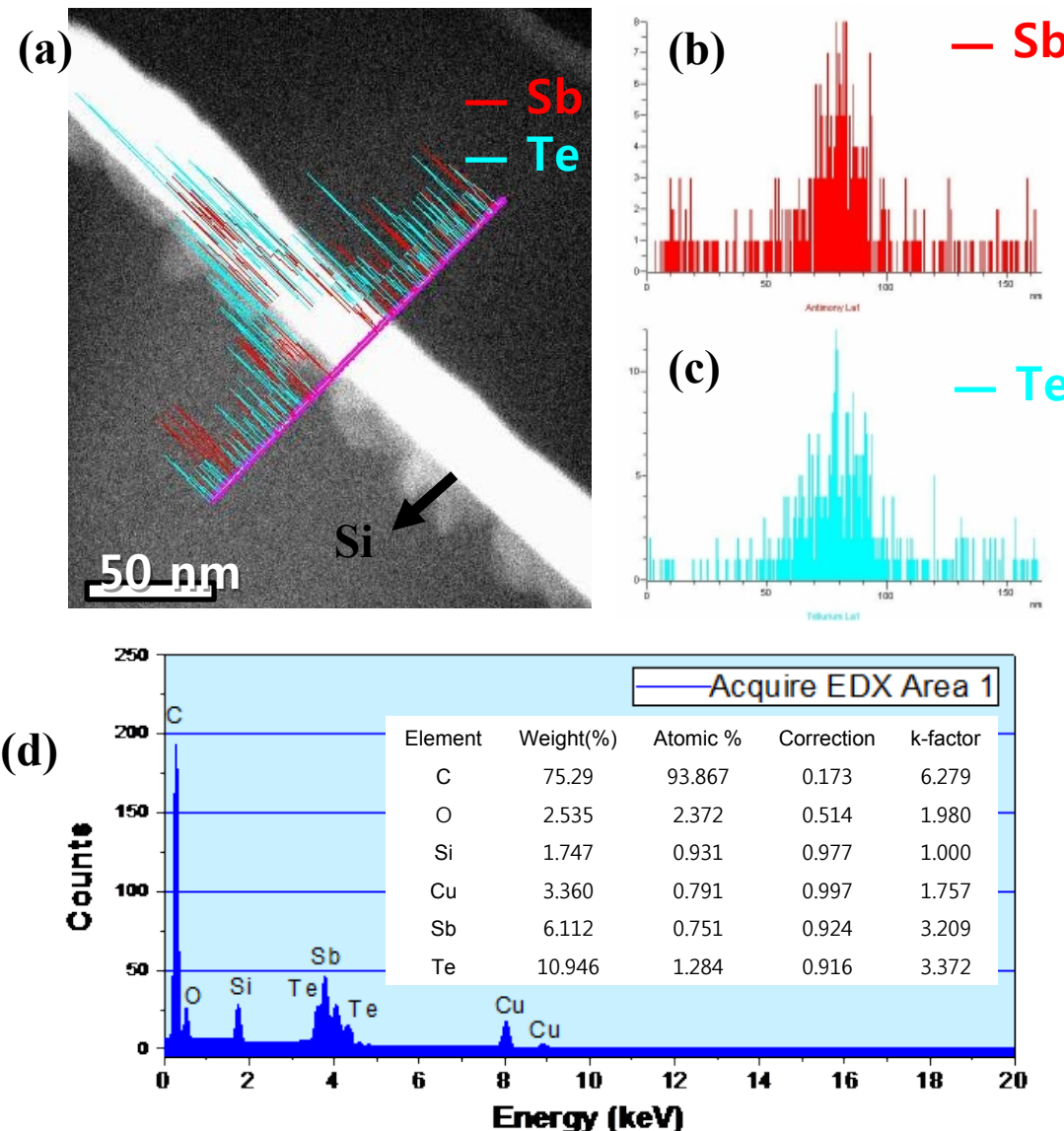
Supporting information S2.HR-TEM images of an annealed thin film at (a) 100 °C, (b) 135 °C, (c) 175 °C, (d) 200 °C and (e) 250 °C. As the annealing temperature increased, the $\{(Sb(3\text{\AA})/Te(9\text{\AA})\}_n$ thin film changes into a Sb₂Te₃ single crystal phase. (f) Enlarged view of the boxed in (e). Consequently, (f) reveal well-ordered Sb₂Te₃ layers and distinct interfaces.

Supporting information S3.



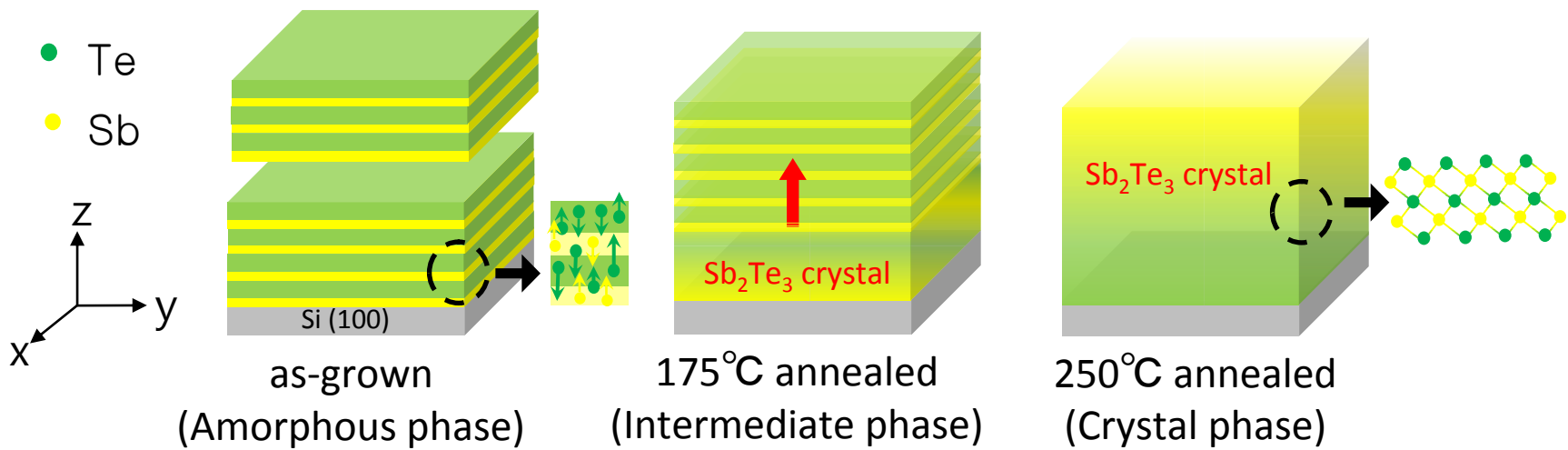
Supporting information S3. Cross-sectional high-resolution transmission electron microscopy (HRTEM) images of our representative 250 °C annealed Sb₂Te₃ thin film on SiO₂/Si(100). (a) An overall view of a Si substrate. (b) Enlarged view of the boxed region in (a). An amorphous interface layer of ~2 nm, and a 50 nm Sb₂Te₃ thin film. (c)-(e) Expanded views of regions (c),(d) and (e) denoted in (b). (f) Further expanded views of regions in (d). Finally, (f) reveal well-ordered Sb₂Te₃ layers and distinct interfaces without any dint. (h) SAED patterns of the boxed region in (f). Moreover, (h) and (i) show that SAED patterns are perfectly well-matched with simulated Sb₂Te₃ SAED patterns.

Supporting information S4.



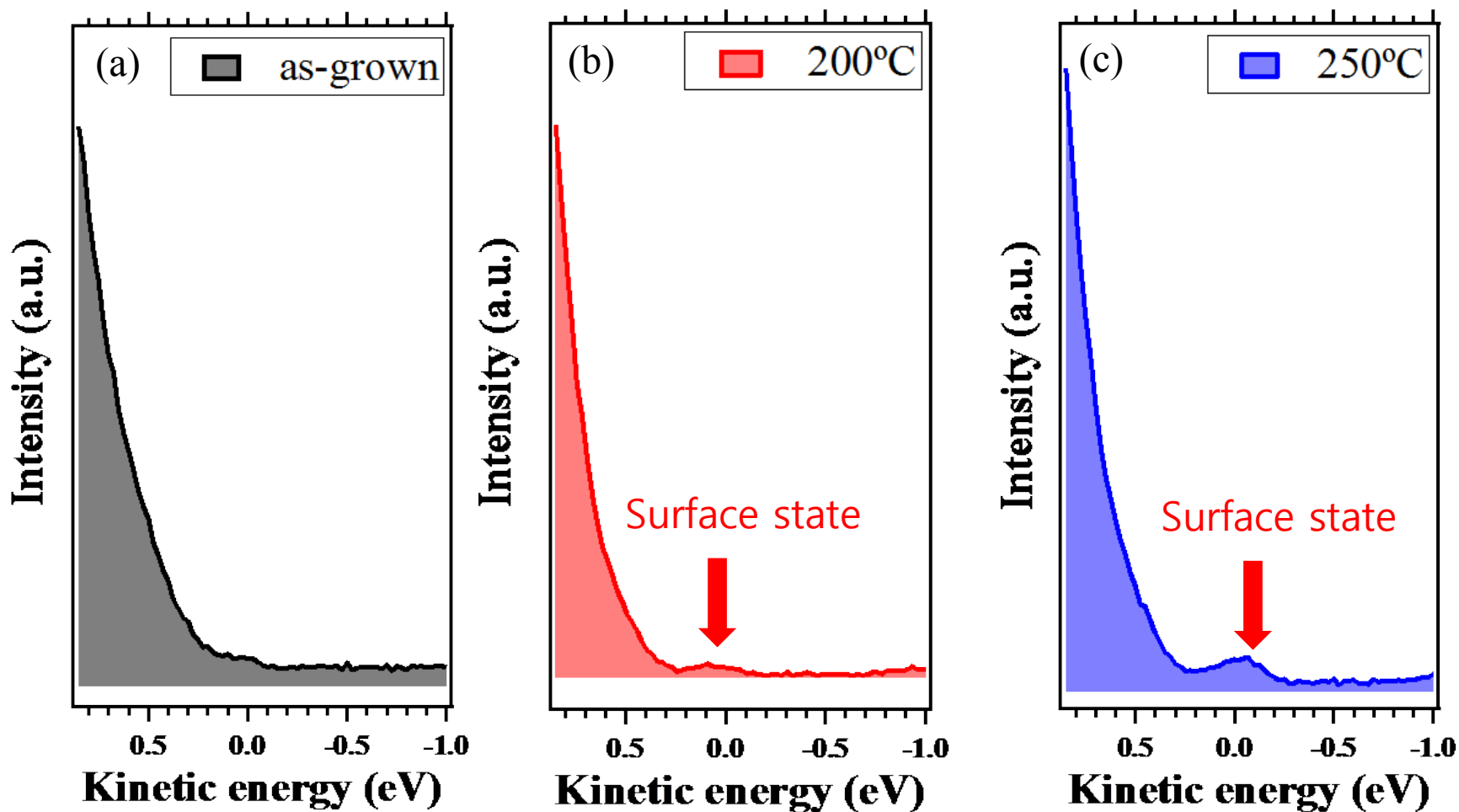
Supporting information S4. EDS element line profile data of (a) all displayed elements, (b) Sb and (c) Te element in 250 °C annealed thin film. As a result, we observed the formation of the single crystalline Sb_2Te_3 thin films in 250 °C annealed thin film in (d) spectra.

Supporting information S5.



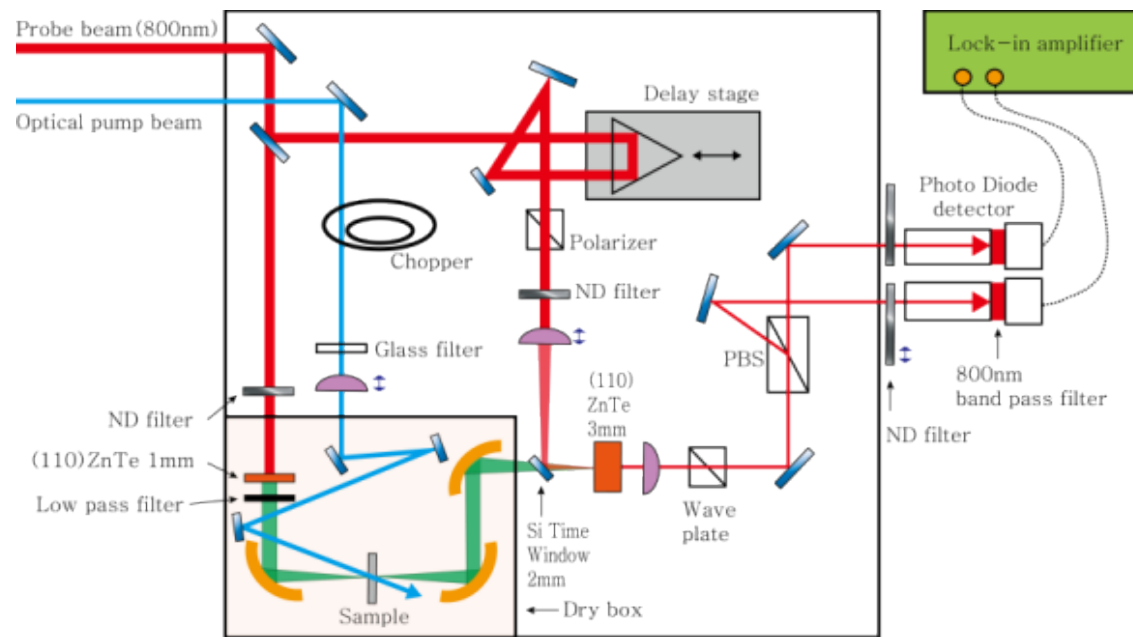
Supporting information S5. Schematic illustration of the change in the alternately layered structure during the annealing process through the inter-diffusion between the Sb and Te layers.

Supporting information S6.



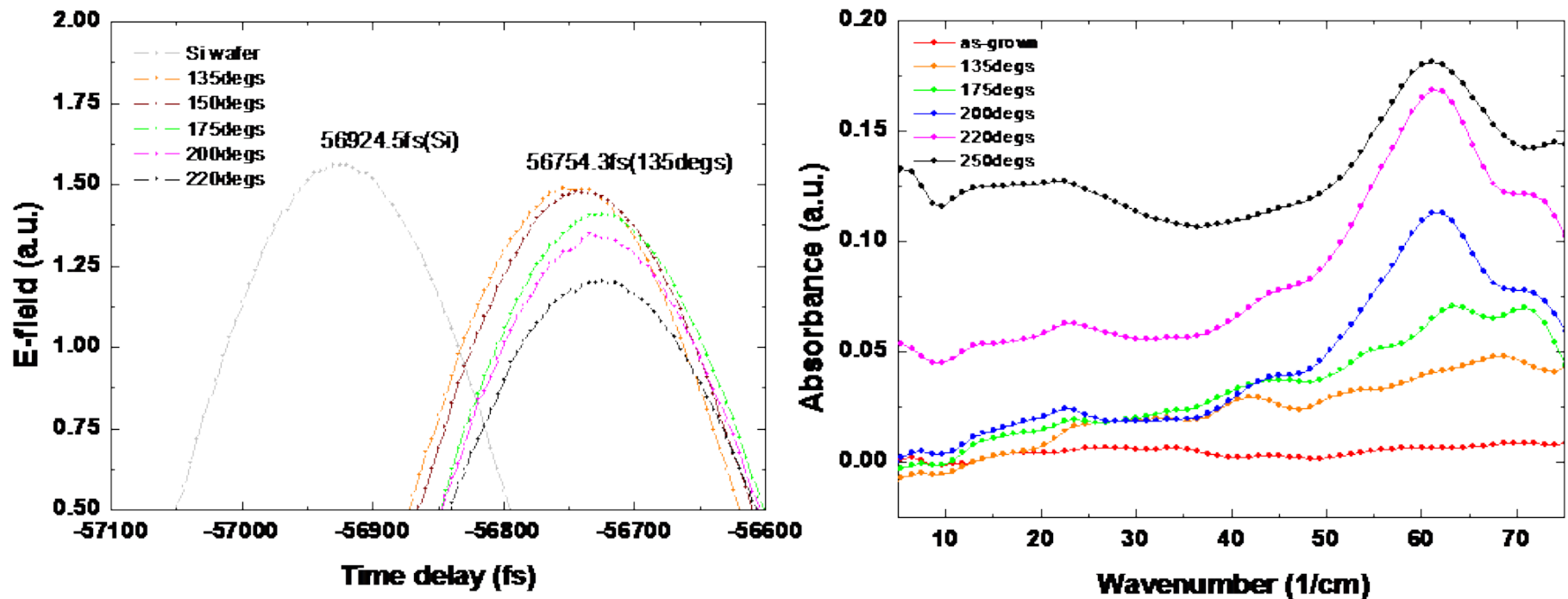
Supporting information S6. Valence band spectra as a function of annealing temperature in $\{\text{Sb}(3\text{\AA})/\text{Te}(9\text{\AA})\}_n$ films. (a) as-grown, (b) 200 °C annealed thin film (c) 250 °C annealed thin film.

Supporting information S7.



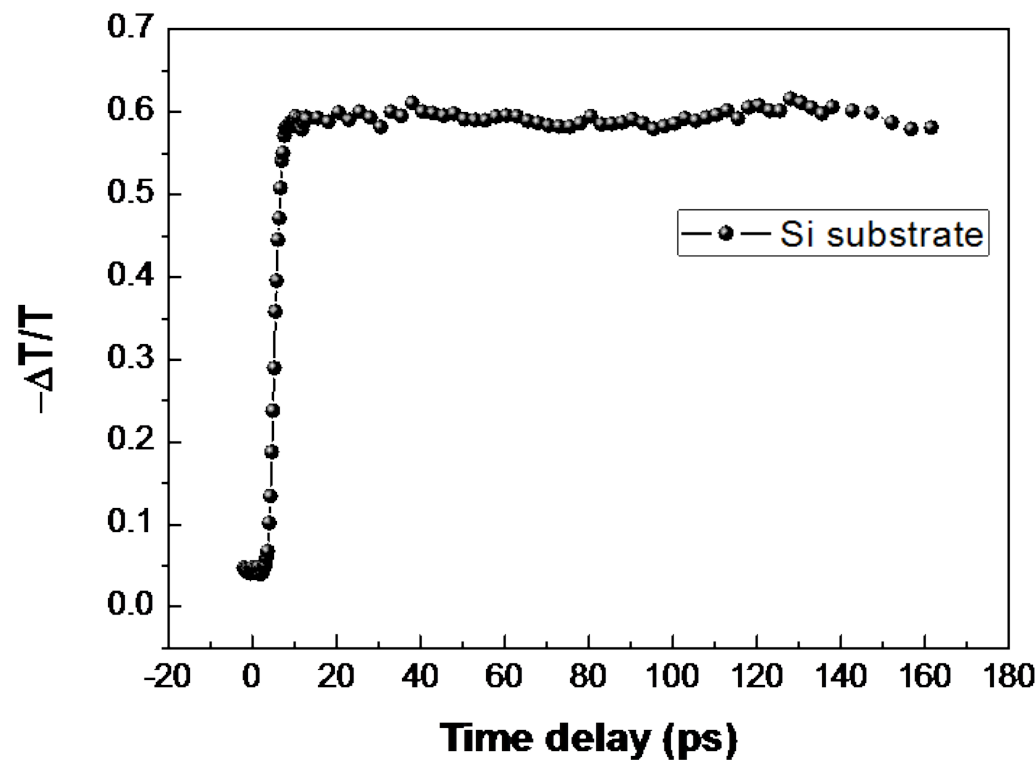
Supporting information S7. Schematic sketch of an electro-optic sampling detection in THz-TDS and OOPTP setup.

Supporting information S8.



Supporting information S8. (a) THz electric field transmitted through reference and our $\{\text{Sb}(3)\text{Te}(9)\}_n$ film series. (b) absorbance spectra of each annealed thin film.

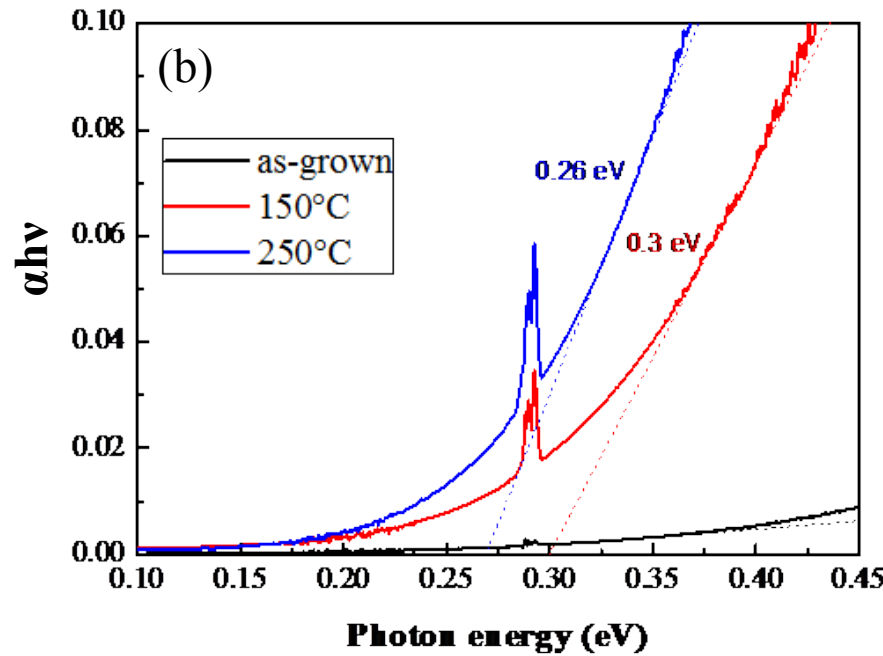
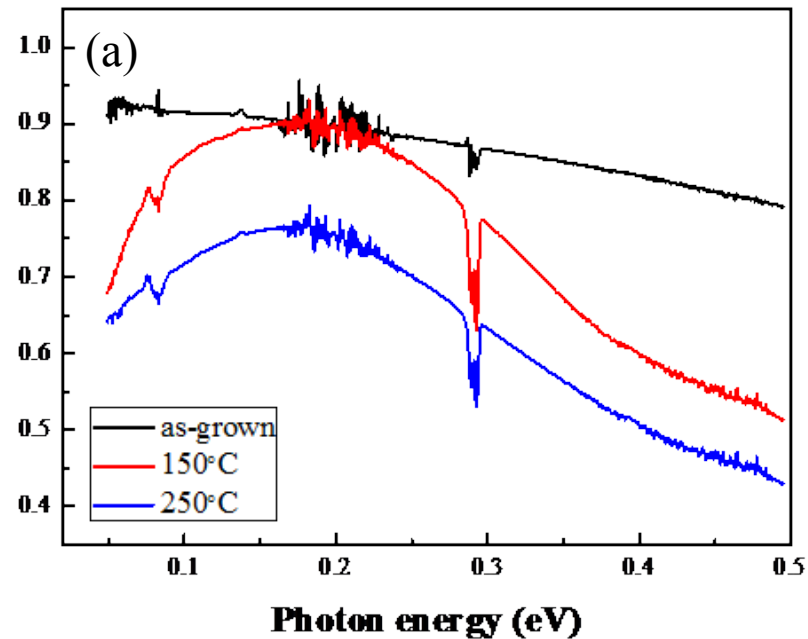
Supporting information S9.



Supporting information S9. OPTP spectra of Si substrate.

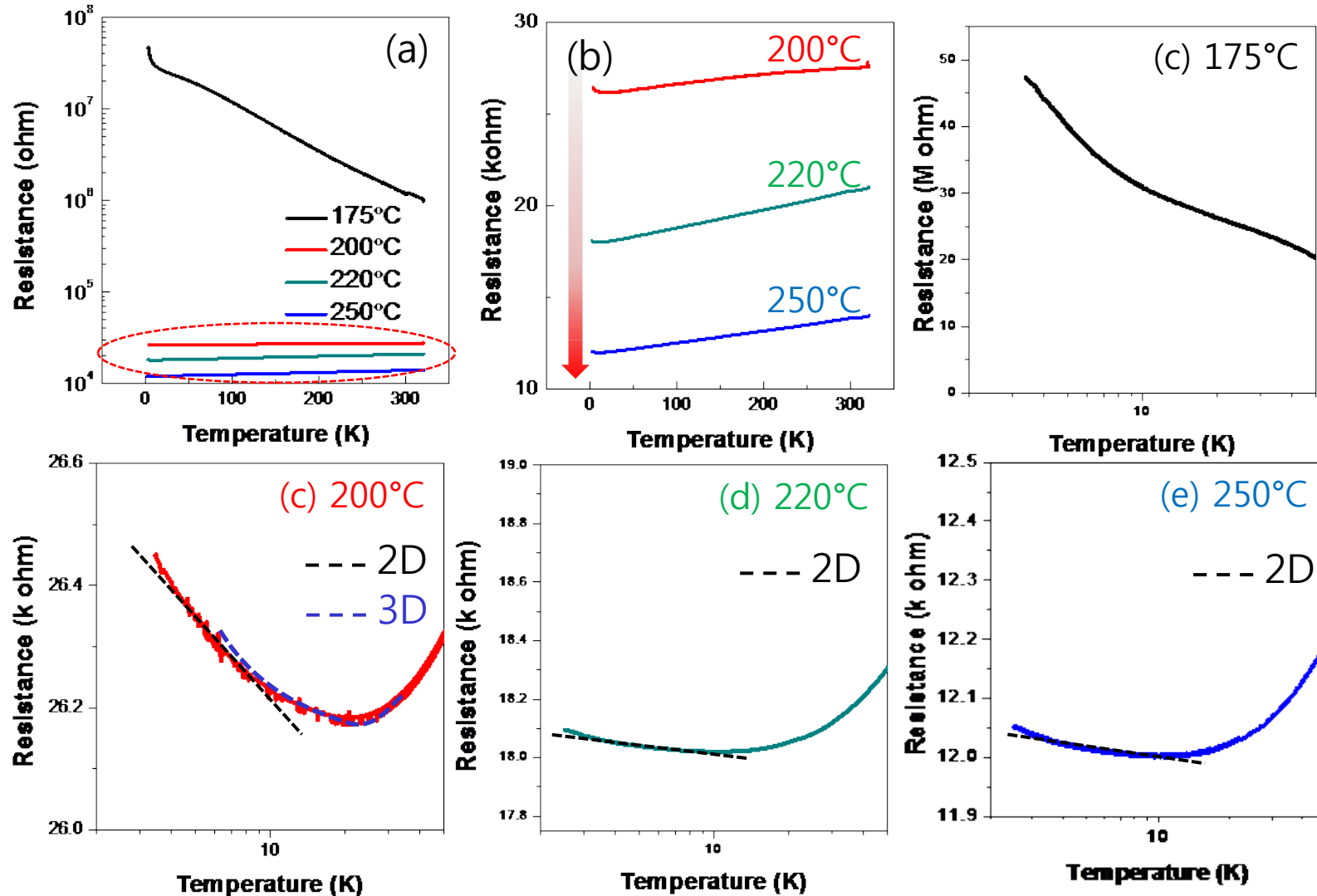
Supporting information S10.

Transmittance



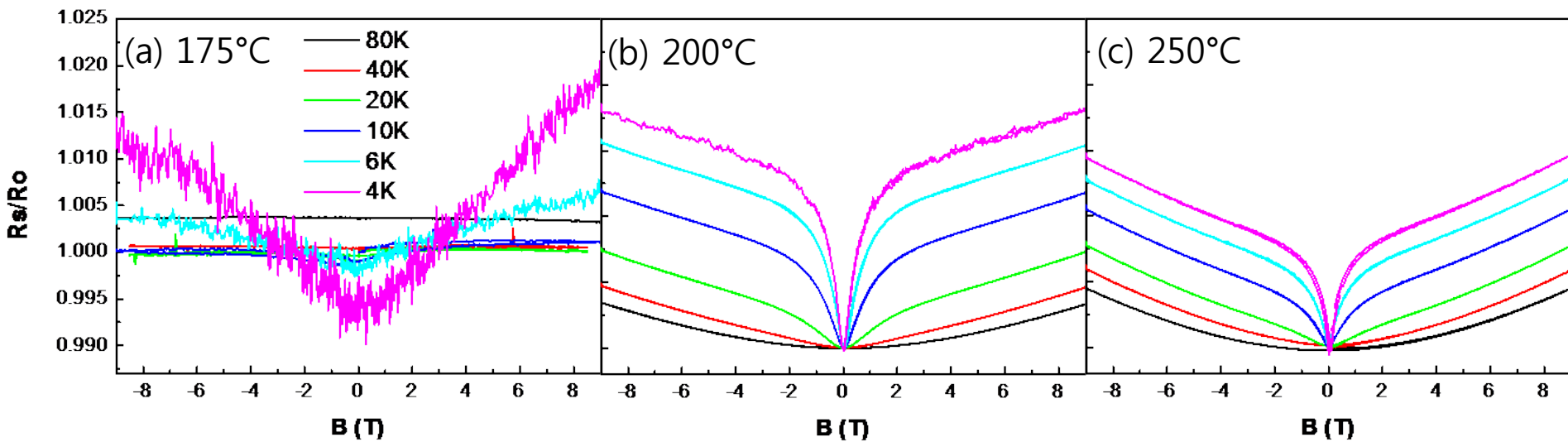
Supporting information S10. FT-IR spectra of (a) transmittance and (b) Tauc plot of $\{\text{Sb}(3)/\text{Te}(9)\}_n$ film series

Supporting information S11.



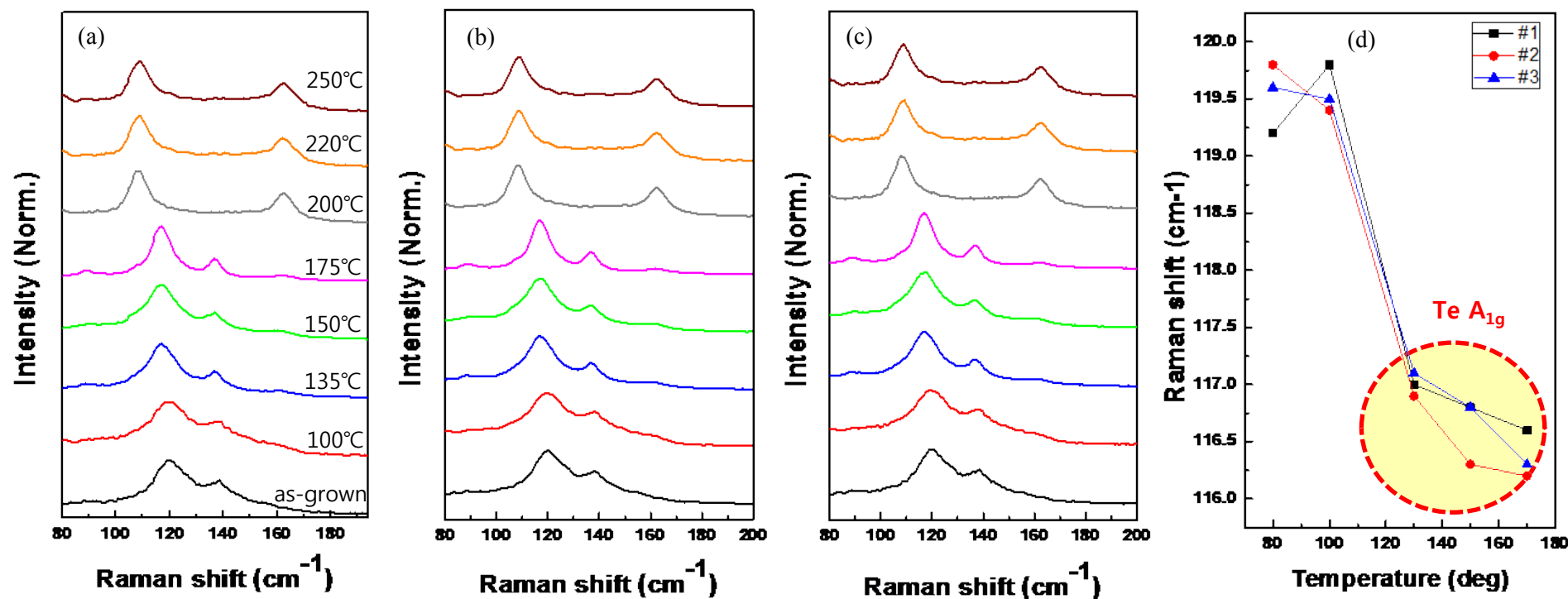
Supporting information S11. Temperature-dependent R_s from 300 to 2K for 175 °C, 200 °C , 220 °C and 250 °C annealed thin films. 175 °C anneal thin film shows the insulating behavior. However, 200 °C , 220 °C and 250 °C annealed thin film show that metallic behavior is enhanced in low temperature .

Supporting information S12.



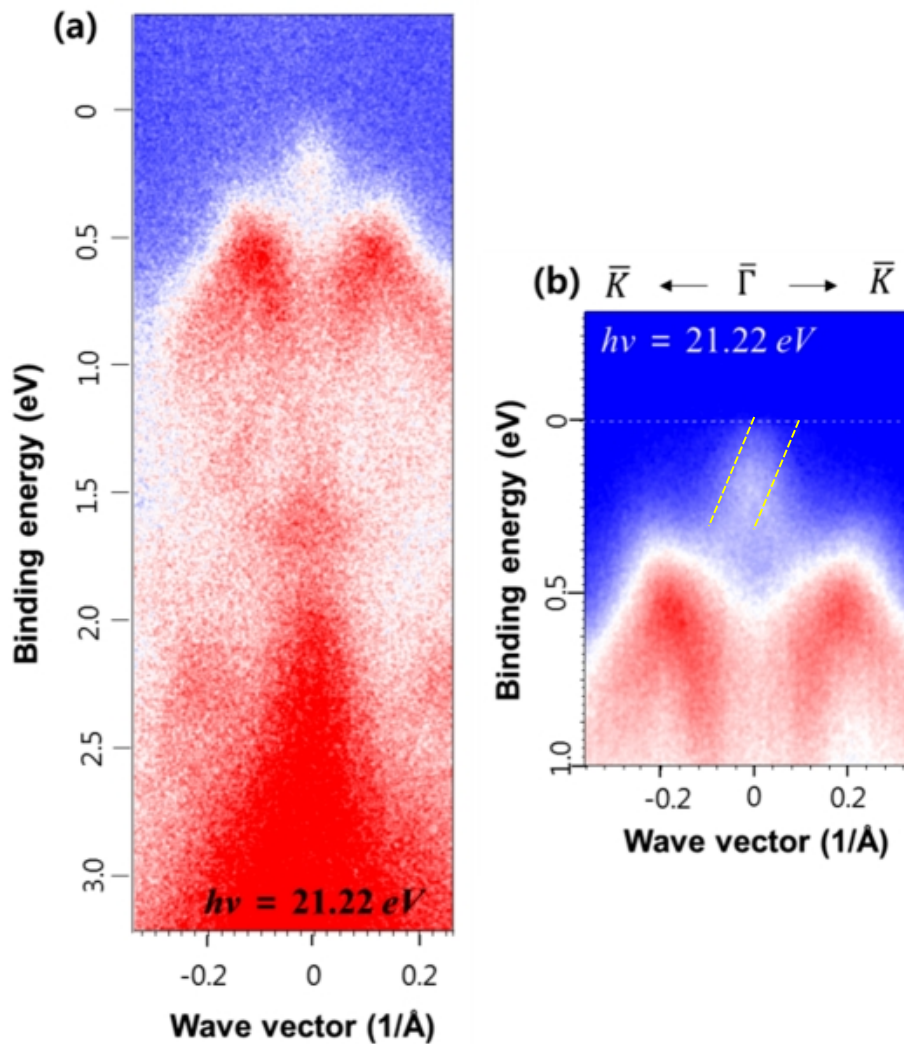
Supporting information S12. Magnetic field dependence of resistance at (a) 175 °C (b) 200 °C and (c) 250 °C annealed thin film. (temperature ranging from 4K to 80K). Deep cusp in low field regime is characteristic of the WAL effect. As annealing temperature increased, shape of weak antilocalization effect was clearly increased.

Supporting information S13.



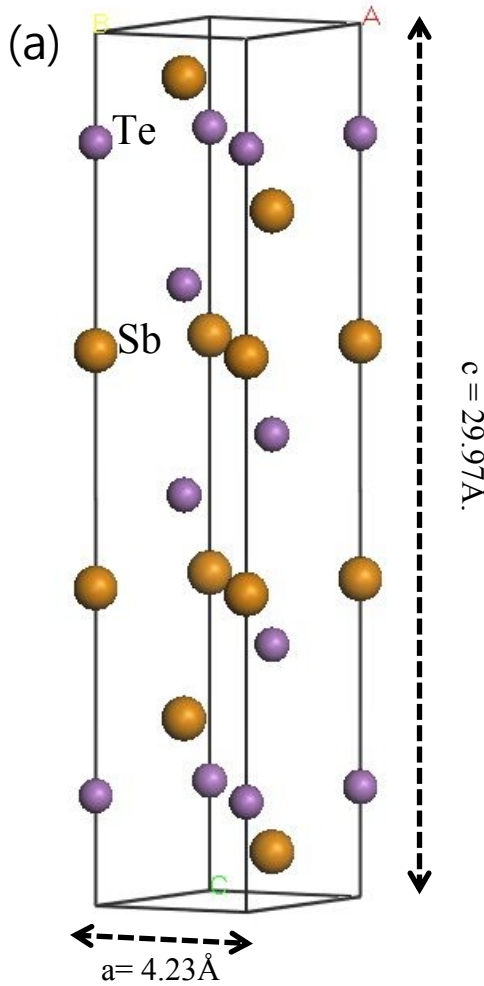
Supporting information S13. Raman spectra of each annealed thin film. (a) 1st spectra, (2) 2nd spectra, (3) 3rd spectra of our thin film series. (d) Temperature dependence of Te A_{1g} phonon mode. From the reproducibility of Raman spectra, red-shift of Te A_{1g} phonon mode confirmed in our sample series.

Supporting information S14.



Supporting information S14. ARPES spectra of 50 nm thick crystalline films. (a) ARPES map taken using He I ($h\nu = 21.22 \text{ eV}$) photons. (b) Sb_2Te_3 film $\bar{\Gamma}\bar{K}$ along directions.

Supporting information S15.



(b)

Sb ₂ Te ₃ crystal structure				
h	k	l	d (Å)	2-theta (°)
0	0	3	9.9867	8.85
0	0	6	4.9933	17.76
0	0	9	3.3289	26.78
0	1	5	3.1362	28.46
0	0	12	2.4967	35.97
0	0	15	1.9973	45.41

$$\text{Hexagonal structure : } \frac{1}{d_{hkl}^2} = \frac{4}{3a^2} (h^2 + hk + k^2) + \frac{l^2}{c^2}$$

$$(hkl) = (003) \quad \frac{1}{9.98^2_{003}} = \frac{4}{3a^2} (0^2 + 0 + 0^2) + \frac{3^2}{c^2} = \frac{9}{c^2} \rightarrow c^2 = 896.40, c = 29.97$$

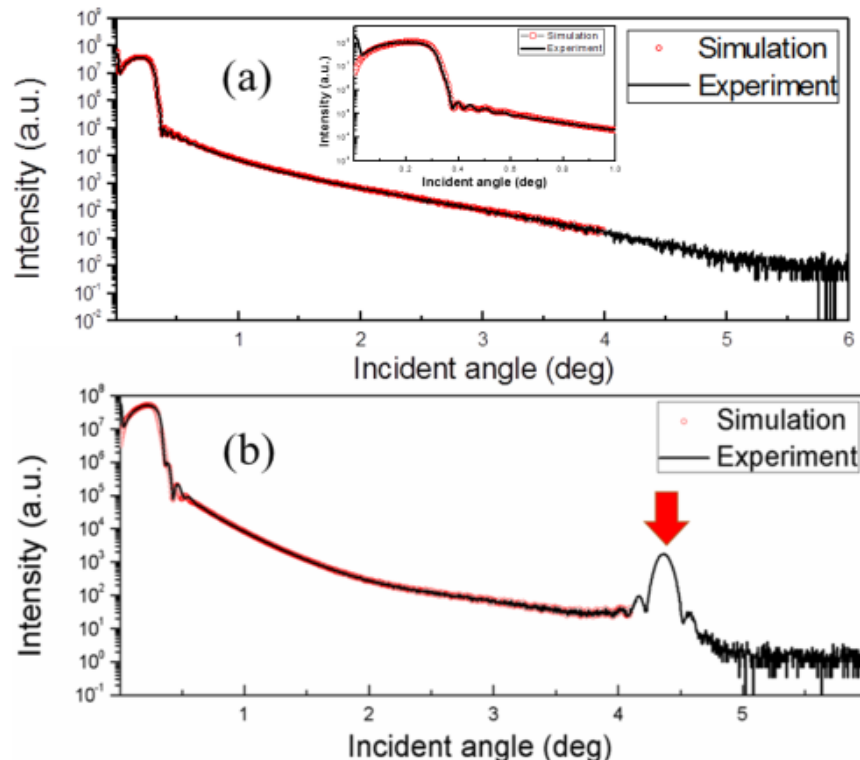
$$(hkl) = (009) \quad \frac{1}{3.32^2_{009}} = \frac{4}{3a^2} (0^2 + 0 + 0^2) + \frac{9^2}{c^2} = \frac{81}{c^2} \rightarrow c^2 = 892.81, c = 29.88$$

$$(hkl) = (015) \quad \frac{1}{3.13^2_{015}} = \frac{4}{3a^2} (0^2 + 0 + 1^2) + \frac{5^2}{c^2} = \frac{4}{3a^2} + \frac{25}{c^2} \rightarrow a^2 = 17.93, a = 4.23$$

Lattice parameters of Sb₂Te₃ crystal structure $a = 4.23\text{\AA}, c = 29.97\text{\AA}$

Supporting information S15. (a) Primitive cell of Sb₂Te₃ hexagonal structure. (b) XRD patterns of 250 °C annealed thin film and calculation of lattice constant in Sb₂Te₃ crystal structure. As a result, we obtained $a = 4.23\text{\AA}$, $c = 29.97\text{\AA}$.

Supporting information S16.



	Layer	Density (g/cm ³)	Thickness (Å)	Roughness (nm)	Repeat
as-grown	Sb	6.24	3.3	2.71	42
	Te	5.15	8.5	2.69	42
	Sb ₂ O ₃	6.11	1.6	5.39	1
crystalline	Sb ₂ Te ₃	6.26	490.68	5.38	1
	Sb ₂ O ₃	6.88	0.22	4.82	1

Supporting information S16. X-ray reflection curves for (a) as-grown and (b) 250 °C annealed thin film. XRR measurement was carried out to measure the reflection under (003) direction. The results showed that the near 4.43° peak was detected because 250 °C annealed thin film was completely crystallized to Sb₂Te₃ hexagonal structure. The red arrows mark the reflection peak of (003) direction.

Supporting information T1.

Supporting information T1. Hall measurements of each annealed thin film.

Major carrier type was maintained with phase transition process.

	Major carrier type	Bulk Concentration (1/cm ³)	Resistivity (Ωcm)	Conductivity (1/Ωcm)	Mobility (cm ² /Vs)
as-grown	P	7.78 - 8.01E+19	0.014 ± 0.0002	67.96 ± 0.98	5.38 ± 0.05
130°C	P	1.16 – 2.32E+19	0.0062 ± 0.002	180.96 ± 6.32	6.50 ± 0.06
150°C	P	6.14 – 7.00E+19	0.0071± 0.0004	139.70 ± 9.14	13.29 ± 0.12
175°C	P	4.78 – 5.52E+19	0.0045± 0.0003	222.23 ± 1.59	26.97 ± 0.24
200°C	P	8.89 – 9.55E+18	0.0045± 0.0001	235.35 ± 8.4	159.54 ± 1.48
220°C	P	9.14 – 10.8E+18	0.0038± 0.0003	259.20 ± 2.15	162.49 ± 1.20
250°C	P	9.60 – 11.0E+18	0.0037± 0.0002	267.80 ± 1.82	162.50 ± 1.23